Dual-Wavelength Polarimetric Radar Analysis of the May 20th 2013 Moore, OK, Tornado

Alexandra Fraire Borunda
California State University Fullerton, Fullerton, CA

Casey B. Griffin and David J. Bodine
Advanced Radar Research Center, University of Oklahoma, Norman, OK

ABSTRACT

The 20 May 2013 Moore, Oklahoma, Tornado was rated as an EF-5 on the Enhanced Fujita scale. Its destructive display of power claimed the lives of 24 people that laid in its path as well as further impacting the local population with damaging winds, large hail and billions of dollars in damage. Because of the tornado's close proximity to multiple radars in the Oklahoma City metro, it provides an opportunity to better understand the scattering characteristics and the dynamics of tornadic debris signatures at different wavelengths. The two radars compared in this research are the PX-1000 that operates at X-band and the KCRI radar that operates at S-band. By comparing the S -and X-band with histograms, box and whisker plots and plan position indicators (PPI) differences in scattering can be seen. While comparing reflectivity, it is seen that S-band is higher than X-band. S-band exhibits more negative values of differential reflectivity as well as lower and more variable values of correlation coefficient.

1. INTRODUCTION

Both radars used in this research project have dual-polarization capabilities. The difference between conventional or single-polarization and dual-polarization radars is the direction in which the electromagnetic (EM) radiation is emitted. A conventional or single polarization radar only sends out an electromagnetic pulse in the horizontal direction and stays parallel to the ground. On the other hand, dual-polarization radars send an electromagnetic (EM) pulse in the horizontal and vertical directions simultaneously. Dual-polarization is preferred when studying tornadic debris because polarimetric variables can add to our understanding of the size, shape, and orientation of debris being lofted within a tornado.

Corresponding author address: Alexandra F. Borunda, California State University Fullerton, 800 N State College Blvd, Fullerton, CA 92831.
email: afborunda@csu.fullerton.edu

A tornadic debris signature (TDS) (Figure 1) is caused by lofted debris within a tornado and is seen on a plan position indicator (PPI) as low to high reflectivity Z_{hh}, low correlation coefficient ρ_{hv}, and low differential reflectivity Z_{DR} (Ryzhkov et al. 2005). Previous TDS studies (Schultz et al. 2012; Van Den Broeke 2015; Houser et al. 2016) provide a better understanding of the type of debris within a tornado and how it relates to the dynamics of the tornado and its parent storm. TDSs can confirm the presence of a tornado (Ryzhkov et al. 2005; Kumjian et al. 2008) and can be related to the possible strength and damage severity of the tornado in real time (Bodine et al. 2013). Knowledge of scatterer characteristics may help mitigate velocity errors caused by debris centrifuging (Dowell et al. 2005; Bodine et al. 2016). Dual-wavelength analyses may be able to provide information necessary to facilitate error mitigation (Bodine et al. 2014).

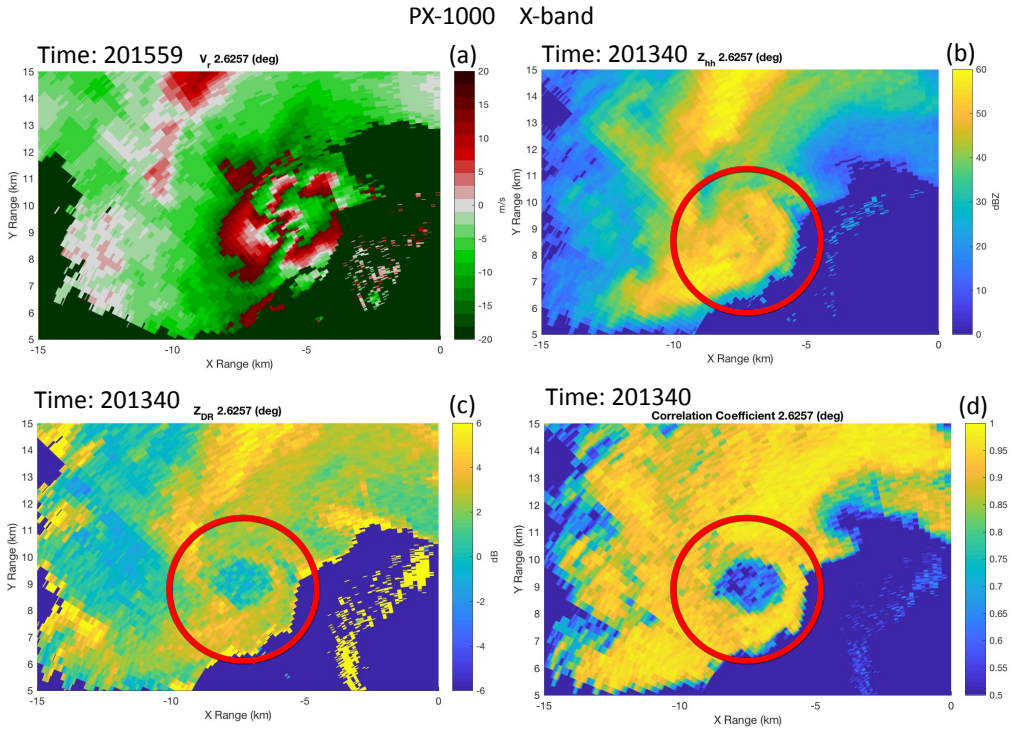

Figure 1. Tornadic Debris Signature (TDS) examples from PX-1000 measured in X-band. Doppler velocity is shown in (a), and a tornado vortex signature can be seen. TDSs are seen as high reflectivity (Z_{hh}) (b), differential reflectivity (Z_{DR}) values that are near zero (c), and low correlation coefficient (ρ_{hv}). These TDSs are evidence that the Moore tornado has touched the ground at time 201340 UTC. These signatures continue throughout the tornadoes lifespan until it dissipates and can no longer loft the debris.

The storm that produced the 20 May 2013 Moore, Oklahoma tornado formed just north of Newcastle, Oklahoma, and began to strengthen and form a striking hook echo; finally, tornadogenesis occurred around 1956 UTC (Kurdzo et al. 2015). Previously, Bodine et al. (2014) compared S- and C-band observations of the tornadic debris signature produced by the 10 May 2010 Moore, Oklahoma EF-4 tornado. Bodine et al. (2014) found that Z_{hh} and ρ_{hv} were higher at S band compared to C band in observations. Z_{hh} was also found to be higher in the S band using the T-matrix algorithm. Lastly, Bodine et al. (2014) found that Z_{hh} decreased with height at C band. This study extends the work of Bodine et al. (2014). using a comparison of X and S band data.

This study investigates the tornadic debris signature characteristics of the 20 May 2013 Moore, Oklahoma, tornado using differential reflectivity (Z_{DR}), velocity (V_r), reflectivity (Z_{hh}) and correlation coefficient (ρ_{hv}). Data from KCRI, which operates at S-band, and PX-1000, which operates at X-band, are used. These radars are co-located near the Norman airport, which makes our polarimetric data from the KCRI and PX-1000 easy to compare. Additionally, PX-1000 can scan at a single elevation every 20 seconds, minimizing the difference in scan times between KCRI and PX-1000.

2. DATA AND METHODS

a. Radar Data

The PX-1000 is a trailer-based, dual-polarization radar that operates in the X band with a wavelength of 3 cm and 2.0° effective beamwidth capable of custom

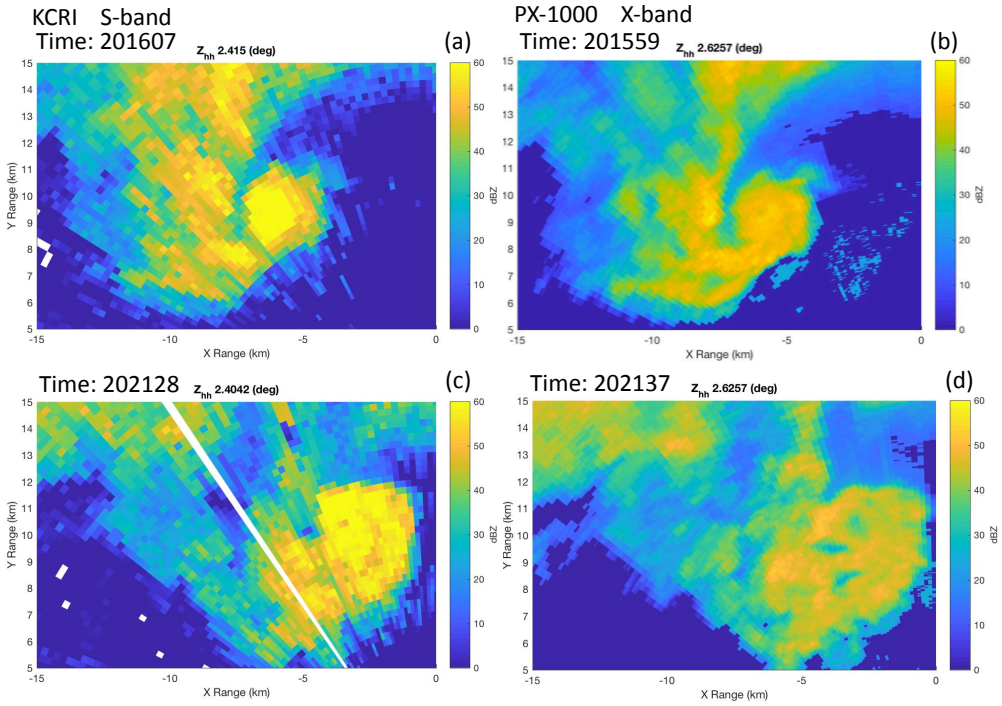

Figure 2. Reflectivity (dBZ) plan position indicators (PPIs) of tornadic debris signatures (TDSs) from (left) KCRI, measured at S band and (right) PX-1000 measured at X band. Scans are valid at (a) 201607 (b) 201559 (c) 202128 and (d) 202137 UTC.

scanning strategies (Cheong et al. 2013; Kurdzo et al. 2014). For this project, the PX-1000 data were reprocessed using pulsed-pair processing rather than multi-lag processing to aid in the comparison to KCRI. KCRI is a dual-polarization test-bed radar run by the National Weather Service Radar Operations Center. It is located at the Max Westheimer airport in Norman, OK and operates in the S-band with a wavelength of 10 cm. For the 20 May 2013 case, PX-1000 was also located at the Max Westheimer airport, making direct volumetric comparisons between PX-1000 and KCRI possible. Attenuation and differential attenuation correction are applied to the data using the method outlined in Bringi et al. (1990); however, values of differential phase (Φ_{DP}) were small in the vicinity of the TDS and thus corrections were small in the region of interest. This small difference had little impact on comparisons for the TDSs and statistical analysis.

b. TDS Identification and Statistical Analysis

The TDS was identified and statistical comparisons were performed on the data similar to those outlined in Bodine et al. (2014). Inside of the radius of maximum wind (RMW), all data were retained for analysis. For distances d from the center of the tornado, where:

$$RMW < d < 2*RMW \quad (1)$$

Debris were identified by $Z_{hh} > 20$ dBZ and $\rho_{HV} < 0.82$. The RMW was approximated to be 0.75 km. The subset data from KCRI and PX-1000 are plotted in histograms and box plots for comparison.

Table 1. (a)

Times	201559	201607
Radar	PX-1000	KCRI
ZDR mean	0.03	-1.6
ZDR median	-0.1	-1.8
ZDR 25	-0.8	-3.9
ZDR 75	0.7	0.8
ZDR 90	1.5	2.5
ZHH mean	45.2	52.8
ZHH median	49.0	54.5
ZHH 25	41.6	47.5
ZHH 75	51.0	60.5
ZHH 90	52.1	62.0
RHO mean	0.64	0.44
RHO median	0.64	0.42
RHO 25	0.58	0.27
RHO 75	0.70	0.59
RHO 90	0.76	0.72

Table 1. (b)

Times	202137	202128
Radar	PX-1000	KCRI
ZDR mean	-0.2	-3.2
ZDR median	-0.3	-3.7
ZDR 25	-0.9	-5.5
ZDR 75	0.4	-1.6
ZDR 90	1.1	1.4
ZHH mean	44.7	55.3
ZHH median	45.4	58.5
ZHH 25	43.3	54.5
ZHH 75	47.1	60.3
ZHH 90	48.3	61.5
RHO mean	0.63	0.43
RHO median	0.63	0.41
RHO 25	0.57	0.29
RHO 75	0.69	0.54
RHO 90	0.75	0.65

Table 1. Tables comparing the mean, median, 25th, 75th, and 90th percentile of the polarimetric variables Z_{hh} (dBZ), Z_{DR} (dB), and ρ_{hv} from PX-1000 and KCRI. Table (a) compares 201559 and 201607 UTC. Table (b) compares 202137 and 202128 UTC.

3. RESULTS

a. Reflectivity Comparison

Seen in Figure 2, reflectivity at S-band is much higher than at X-band within the TDS. This could be due to larger debris being lofted, which can cause reflectivity differences to be more drastic. In Figure 3, a noticeable tail trails off to the left of the 25th percentile. This tail of low ρ_{hv} values could possibly be evidence of a debris ejection (Kurdzo et al. 2015), which is classified as an abundance of debris that is being ejected from the tornado's center. A visual example can be seen in Figure 7b where the debris ejection manifests as the trailing tail of values of low ρ_{hv} southwest of the TDS. Debris ejections are hypothesized to be caused by the rear flank gust front or winds within the rear flank downdraft (Kurdzo et al. 2015). In Figure 3a,b there is a visible 10 dB difference between the 90th percentiles of Z_{hh}. Also seen in Figure 3c,d, there is about a 13 dB difference when comparing the 90th percentiles. Values of 90^{th} percentile reflectivity and other polarimetric variables are displayed in Table 1. These dual-wavelength differences could possibly be due to the largest debris being found in the 90th percentile radar volumes and this abundance of large debris could be causing Mie scattering to occur. Mie scattering occurs when the particles within the medium have diameters greater than $\lambda/16$, where λ is the radar wavelength. Since the largest abundance of large debris is found at the 90th percentile, this causes the highest reflectivity differences to be found.

b. Differential Reflectivity Comparison

When analyzing Figure 4, more negative values of Z_{DR} are seen in the 25th percentile at S-band compared to X-band. This great quantity of negative values could be due to a higher power return in the vertical orientation. This implies that on average more of the debris is spending more time in one orientation (probably vertical), as has been noted in observations at S and C bands (Bodine et al. 2014) and in simulated TDSs (Cheong et al. 2017). This observation of negative Z_{DR} values is also seen on the PPI charts in Figure 5a,c. When observing Z_{DR} values at X-band (Figure 6e,f) the overall average of the values were found to be near zero. These near-zero values are well documented in the literature (e.g., Ryzhkov et al. 2005) and are caused by random particle orientation. The KCRI data was found to be relatively evenly distributed at each time (Figure 4a,c). There could be

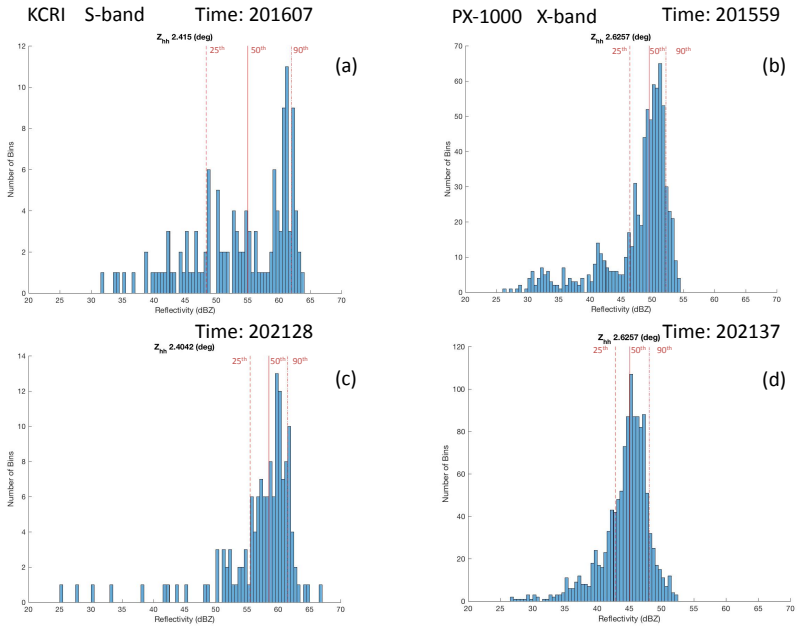

Figure 3. Histograms comparing reflectivity (dBZ) from KCRI (left) and PX-1000 (right). The 25th, 50th and 90th percentiles are represented by red lines. Figures are valid at (a) 201607, (b) 201559, (c) 202128, and (d) 202137 UTC.

many factors contributing to this distribution. One factor could be related to noisier measurements, since there are low values of ρ_{hv} recorded.

c. Correlation Coefficient Comparison

When comparing ρ_{hv} between each wavelength, X-band (Figure 7b,d) is noticeably higher when compared to S-band (Figure 7a,c). This comparison between bands can also be seen in Figure 6. This could possibly be due to Mie scattering. Another possibility is that S-band is being more influenced by debris; the presence of debris causes ρ_{hv} to have smaller values. It is hard to determine the exact reason for low ρ_{hv} since it is a complex variable that is not fully understood. This complexion is due to how ρ_{hv} is affected by the size, shape, and orientation of the debris. Another factor that could contribute to X-band being much higher than S-band is that X-band values could be influenced by rain. X-band is more sensitive to rain and therefore rain can dominate more of the signal (Bodine et al. 2016).

When analyzing the histogram comparisons for ρ_{hv} (Figure 8) there is a notably large difference between distributions of data between the radars. KCRI data appears to be randomly distributed which could be due to noise in the KCRI data (Figure 8a,c). PX-1000 data appears to have a normal distribution (Figure 8b,d). Statistical tests could be used in the future to determine if the polarimetric variables fit a particular type of distribution. The high values of ρ_{hv} at X-band are possibly from raining skewing the data to be higher than at S-band (Figures 8).

Just to note, in Figure 8a,c, the KCRI data stop at a value of 0.2. This is due to an artifact in how the data were written in the NCDC archive. Everything with a value of 0.2 and under is classified with a value of 0.2. Additionally, it is noted that the PX-1000 has more bins than KCRI due to the higher resolution that PX-1000 possesses.

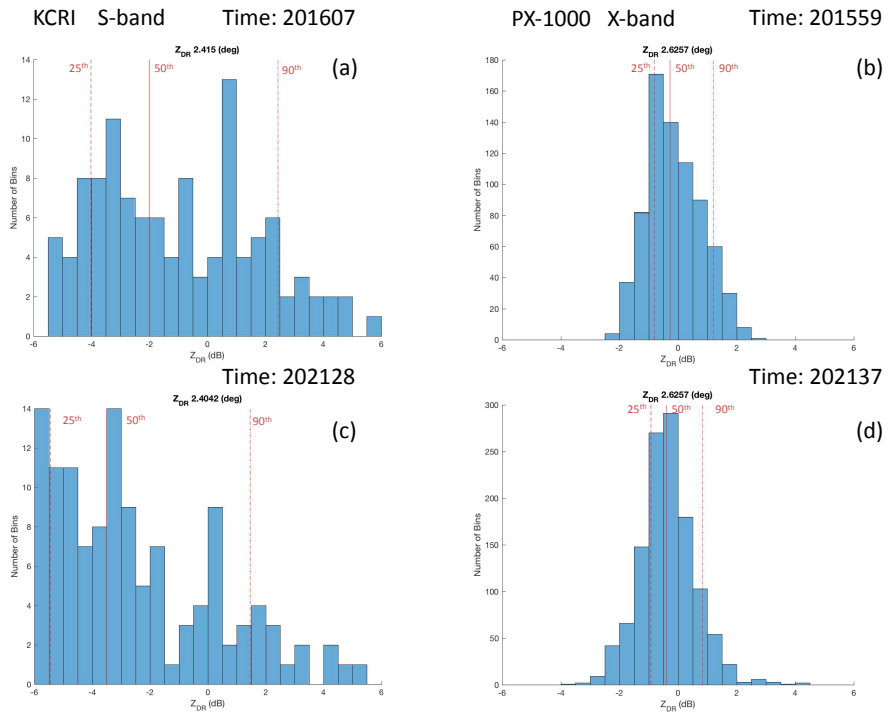

Figure 4. The same as Fig. 3 except for differential reflectivity (dB).

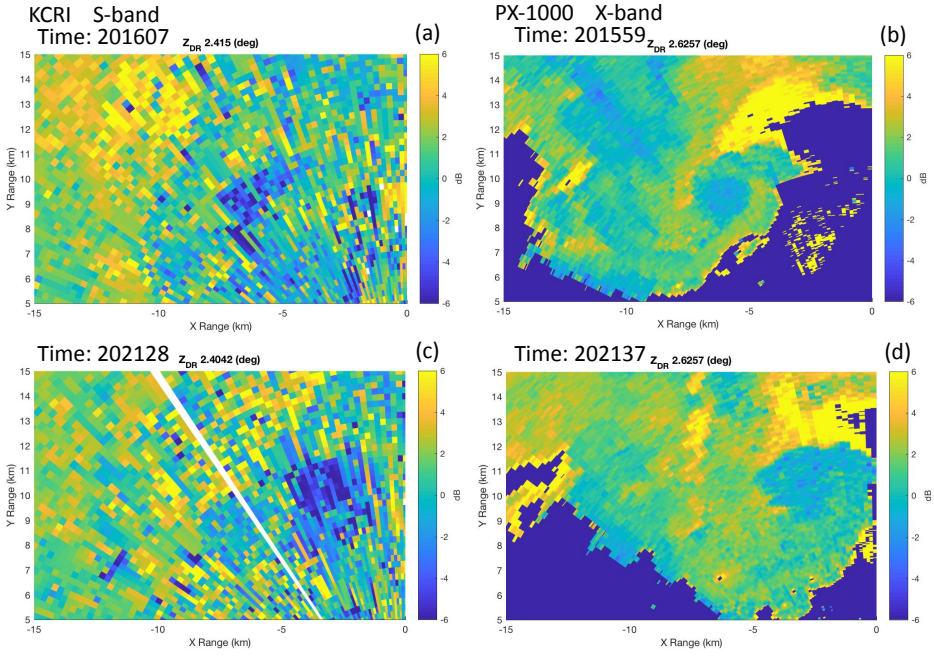

Figure 5. The same as Fig. 2 except for differential reflectivity (dB).

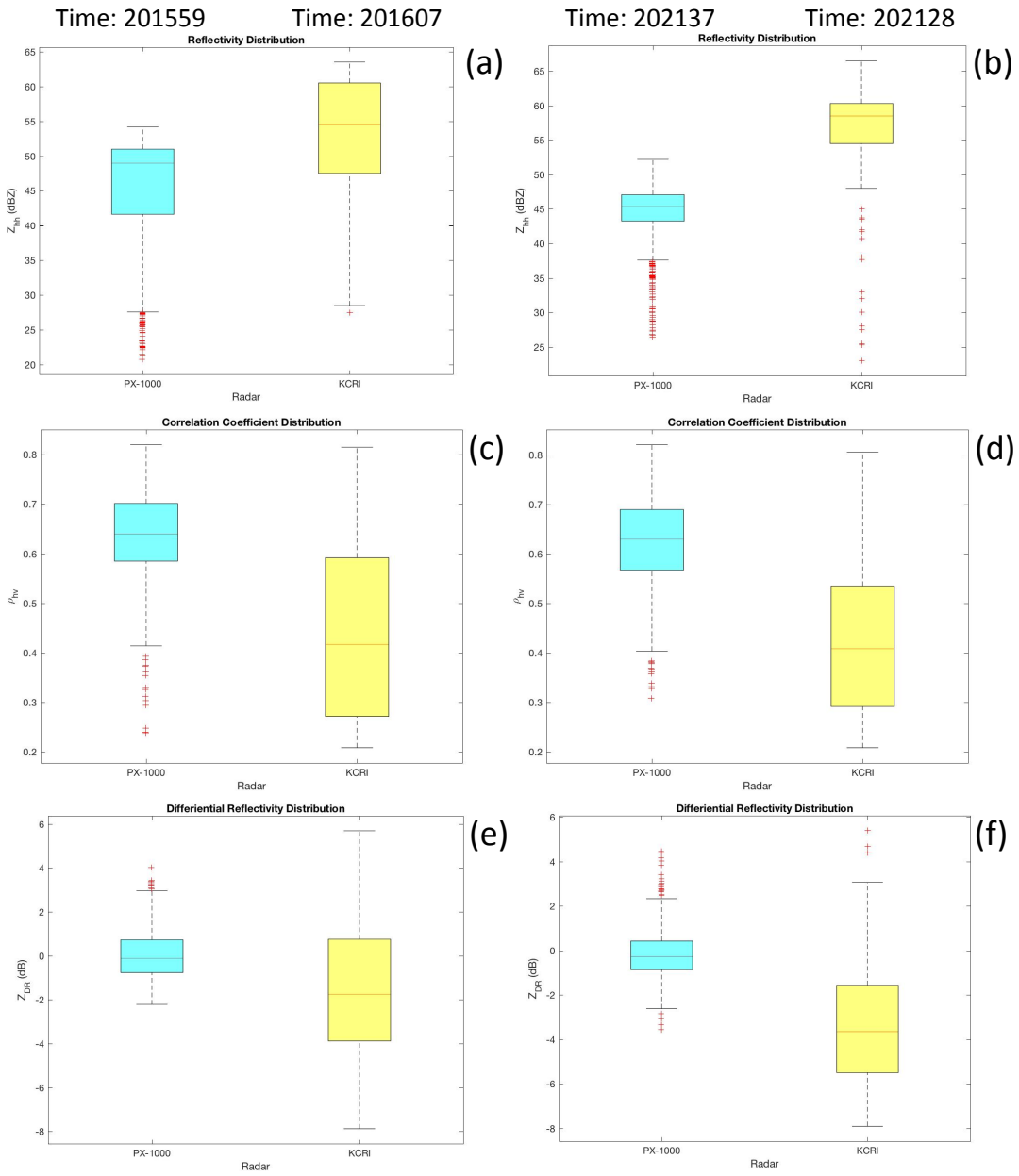

Figure 6. Box and whisker plots for KCRI and PX-1000 representing (a–b) reflectivity (dBZ), (c–d) correlation coefficient, and (e–f) differential reflectivity (dB) at (a,c,e) 201559 UTC for PX-1000 (left), (a,c,e) 201607 UTC for KCRI (right), (b,d,f) 202137 UTC for PX-1000 (left), and (b,d,f) 202128 UTC for KCRI (right).

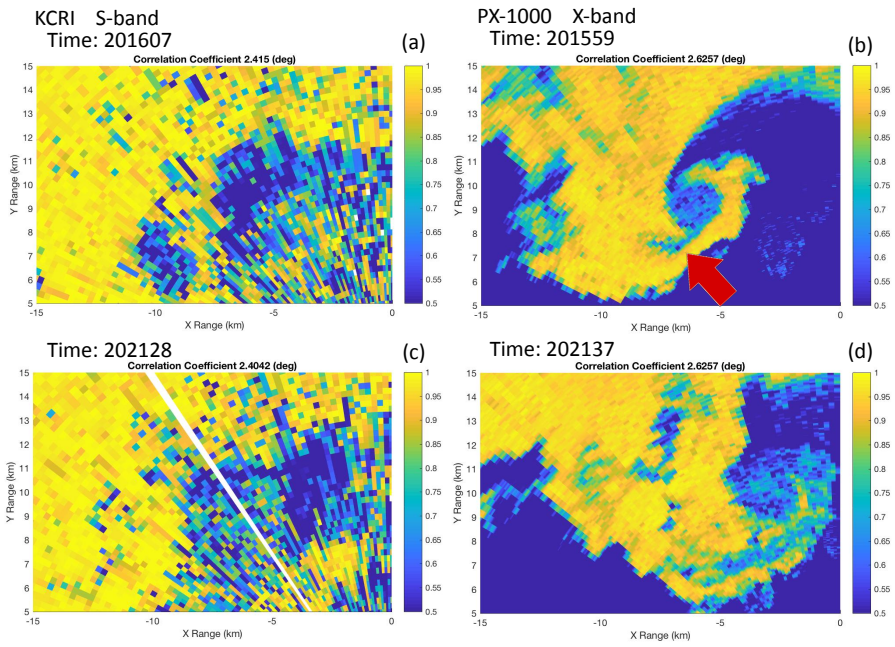

Figure 7. The same as Fig. 2 except for correlation coefficient. The red arrow is pointing to an example of a possible debris ejection can be seen protruding out under the TDS as a tail of low ρ_{hv} values in (b, arrow).

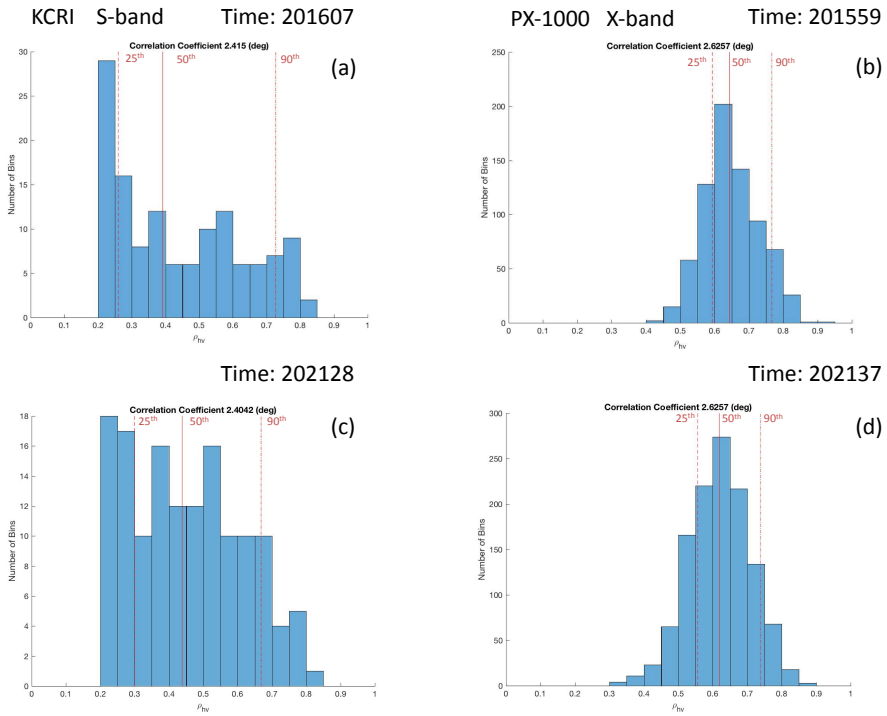

Figure 8. The same as Fig. 3 except for correlation coefficient.

4. DISCUSSION AND CONCLUSIONS

The May 20th Moore, Oklahoma, tornado was a reminder to the local population of Moore that Mother Nature possesses a tremendous amount of strength and that we as a civilization are subjugated to her elusive rules. In order to better understand such events, intensive research comes in to play. Many have conducted previous research on tornado debris signatures, such as Bodine et al (2014), which was the motivation behind this project. Bodine et al (2014), compared S- and C-band radar observations for the 10 May 2010 Moore, Oklahoma, EF-4 tornado. This study extends this research by comparing S- and X- band data from the 20 May 2013 EF-5 tornado, allowing for comparison with the observations in Bodine et al. (2014).

It was found that values of reflectivity at S-band were higher than at X-band. Large, 10 dB/13 dB differences in the 90th percentile values were observed between the two wavelengths at the two compared times. The greatest dual-wavelength differences may indicate the presence of the largest debris. These large reflectivity differences between S and X bands are consistent with T-matrix calculations (Bodine et al. 2016), and are larger than those observed between S and C bands (Bodine et al. 2014). When comparing differential reflectivity, a greater quantity of negative values was found at S-band when compared to X-band. When comparing correlation coefficient, X-band was found to be higher when compared to S-band. It is interesting to note that Bodine et al. (2014) found the opposite with lower correlation coefficient at C band compared to S band. We speculate that the greater influence of rain at X band compared to S band contributed to higher correlation coefficients.

Finally, future investigations expected to be derived from this project include electromagnetic calculations of debris. This is also known as the T-matrix algorithm or laboratory measurements (Bodine et al. 2016; Cheong et al. 2017). Once this algorithm is calculated, the results can be compared with observations from this study. Additionally, GIS maps that compare the results found in this paper, the results from the T-matrix algorithm calculations and the land use from the tornado's track can help identify the types of debris observed in the 20 May 2013 Moore tornado. Future studies of TDS's can improve our understanding of the strength of tornadoes in real time and provide more information about the physical properties of the debris being lofted.

5. ACKNOWLEDGMENTS

This research was funded by the National Science Foundation under Grant No. AGS-1560419. The author would like to thank Daphne LaDue, the Research Experience for Undergraduates (REU) program, and the Advanced Radar Research Center (ARRC) for this opportunity to conduct research. The author would also like to thank Blake James and Alexander Moreno for assistant with coding along the way. Jim Kurdzo and Boon Leng Cheong also provided helpful discussions and assistance with the PX-1000 data. David Bodine is supported by the National Science Foundation under Grant
No. AGS-1303685.

6. REFERENCES

Bodine, D. J., M. R. Kumjian, R. D. Palmer, P. L. Heinselman, A. V. Ryzhkov, 2013: Tornado damage estimation using polarimetric radar. *Weather and Forecasting,* **28,** 139-158.

Bodine, D. J., R. D. Palmer, and G. Zhang, 2014: Dual-Wavelength polarimetric radar analyses of tornadic debris signatures. *Journal of Applied Meteorology and Climatology*, **53**, 242-261.

Bodine, D. J., R. D. Palmer, T. Maruyama, C. J. Fulton, Y. Zhu, and B. L. Cheong, 2016: Simulated frequency dependence of radar observations of tornadoes. *Journal of Atmospheric and Oceanic Technology,* **33,** 1825-1842.

Bringi, V. N., V. Chandrasekar, N. Balakrishnan, and D. S. Zrnic, 1990: An examination of propagation effects in rainfall on radar measurements at microwave frequencies. *Journal of Atmospheric and Oceanic Technology*, **7**, 829-840.

Cheong, B. L., R. Kelley, R. D. Palmer, Y. Zhang, 2013: PX-1000: A solid-state polarimetric X-band weather radar and time-frequency multiplexed waveform for blind range mitigation. *IEEE Transactions on Instrumentation and Measurement*, **62,** 3064-3072.

Cheong, B. L., D. J. Bodine, C. J. Fulton, S. M. Torres, T. Maruyama, and R. D. Palmer, 2017: SimRadar: A polarimetric radar time-series simulator for tornadic debris studies. *IEEE Transactions on Geoscience and Remote Sensing*, **55,** 2858-2870.

Dowell, D. C., C. R. Alexander, J. M. Wurman, and L. J. Wicker, 2005: Centrifuging of hydrometeors and debris in tornadoes: Radar-reflectivity patterns and wind-measurements errors. *Mon. Wea. Rev.,* **133,** 1501-1524.

Houser J. L., H. B. Bluestein, and J. C. Snyder, 2016: A finescale radar examination of the tornadic debris signature and weak-echo reflectivity band associated with a large, violent tornado. *Monthly Weather Review*, **144**, 4101-4130.

Kumjian M. R., and A. V. Ryzhkov, 2008: Polarimetric signatures in supercell thunderstorms. *Journal of Applied Meteorology and Climatology*, **47**, 1940-1961.

Kurdzo J. M., D. J. Bodine, B. L. Cheong, and R. D. Palmer, 2015: High-temporal resolution polarimetric X-band Doppler radar observations of the 20 May 2013, OK, tornado. *Monthly Weather Review*, **143**, 2711-2735.

Ryzhkov, A., T. J. Schuur, D. W. Burgess, and D. S. Zrnic, 2005: Polarimetric tornado detection. *Journal of Applied Meteorology*, **44**, 557-570.

Schultz, C. J., and Coauthors, 2012a: Dual-polarization tornadic debris signatures Part I: Examples and utility in an operational setting. *Electron. J. Operational Meteor*., **13**, 120-137.

Van Den Broeke, M. S., 2015: Polarimetic tornadic debris signature variability and debris signatures. *Journal of Applied Meteorology and Climatology*, **54**, 2389-2405